

TT-Stack: A Transformer-Based Tiered-Stacking Ensemble Framework with Meta-Learning for Automated Breast Cancer Detection in Mammography

1st Showkat Osman
Dept. of ECE

North South University
Dhaka, Bangladesh
showkat.osman@northsouth.edu

2nd Md. Tajwar Munim Turzo
Dept. of ECE

North South University
Dhaka, Bangladesh
munim.turzo@northsouth.edu

3rd Maher Ali Rusho*
NMR Spectroscopist

Lassonde School of Engineering York University
Toronto, Canada
alirusho@yorku.ca

4th Md. Makid Haider
Dept. of EEE

Ahsanullah University of Science and Technology
Dhaka, Bangladesh
makid94haider@gmail.com

5th Sazzadul Islam Sajin
Dept. of ECE

North South University
Dhaka, Bangladesh
sazzadul.sajin@northsouth.edu

6th Ayatullah Hasnat Behesti
Dept. of ECE

North South University
Dhaka, Bangladesh
ayatullah.behesti@northsouth.edu

7th Ahmed Faizul Haque Dhrubo
Dept. of ECE

North South University
Dhaka, Bangladesh
ahmed.dhrubo@northsouth.edu

8th Md. Khurshid Jahan
Dept. of ECE

North South University
Dhaka, Bangladesh
khurshid.jahan@northsouth.edu

9th Mohammad Abdul Qayum
Dept. of ECE

North South University
Dhaka, Bangladesh
mohammad.qayum@northsouth.edu

Abstract—Breast cancer continues to be the second most common cause of cancer-related deaths around the world, with early detection being important to improve survival rates for patients. Traditional computer-aided diagnosis systems have limitations in their ability to represent features and generalize to the range of mammographic images. We present a new two-level Stack of Transformers (TT-Stack) ensemble framework based on using heterogeneous lightweight vision transformer architectures to automatically identify breast cancer in mammograms. Specifically, we integrate seven state-of-the-art vision transformers: RepViT, DaViT, EfficientViT, MobileViT, FasterViT, MViT, and PVT-v2 while also designing a two-tier meta-learning approach for the ensemble by simply taking the logits from the base model and applying logistic regression for binary classification (Cancer vs. Non-Cancer). Each of the transformer backbone models was developed to process single-channel grayscale mammograms while still taking advantage of transfer learning from pre-training on ImageNet so that they would offer a parameter-efficient approach that may reasonably be applied in clinical practice with minimal variance. The training process included stratified 80/20 splits when necessary, class-balanced upsampling, early stopping, and an adaptive learning rate schedule on the public Mammogram Mastery dataset. In separate evaluations here, it was determined that EfficientViT and PVT-v2 were the top performing models achieving 99.33% validation, 97.96% F1-score, and perfect 1.000:0 ROC-AUC with only small train/validation gaps (≤ 0.67 points). Finally, the TT-Stack ensemble model by the end of the evaluation reached 99.33% accuracy with 100% precision, 96% recall, 97.96% F1-score and a 99.97% ROC-

AUC, and demonstrated robustness in performance due to the diversity of the architecture. In comparison with the latest state-of-the-art methods, our framework demonstrates improved performance; for example, TT-Stack achieved above the performance of RadiNet-XGBoost (96.67%) and MedFoundX (98.7%) on the same dataset. The framework also establishes a novel benchmark for transformer-based breast cancer detection while being computationally efficient through lightweight architectures of the method, creating a clear pathway to creating scalable, accurate mammography screening systems, particularly in resource-limited clinical contexts.

Index Terms—Breast cancer detection, Vision transformers, Ensemble learning, Meta-learning, Medical image classification, Mammography, Computer-aided diagnosis, Transfer learning.

I. INTRODUCTION

Bangladesh, with a population of approximately 173.97 million as of 2024 (Worldometer), faces significant health challenges, with nearly half of the population comprising women [1]. Each year, a large number of people suffer from various diseases, with women disproportionately affected due to societal norms that inhibit them from openly discussing health issues. In many cases, women refrain from sharing their medical concerns, even with family members or healthcare providers, fearing stigmatization and being perceived as a burden. As a result, numerous women succumb to preventable conditions due to delayed diagnosis and treatment. Breast

cancer, in particular, stands as one of the most critical health issues faced by women, both globally and in Bangladesh.

Breast cancer is the second leading cause of cancer-related death worldwide. It occurs when breast cells undergo mutations, becoming cancerous and multiplying to form tumours. Although the disease predominantly affects women, especially those assigned female at birth (AFAB) and aged 50 and older, it can also impact men and younger individuals [2]. Approximately 80% of breast cancer cases are invasive, meaning the tumour may spread beyond the breast to other parts of the body [3]. Breast cancer is classified into common and less common types. Common types include invasive ductal carcinoma, lobular breast cancer, and ductal carcinoma in situ. Less common types include triple-negative breast cancer, inflammatory breast cancer, and Paget's disease of the breast [3].

Recognizing the early signs and symptoms of breast cancer is crucial for effective treatment. Common symptoms include changes in breast size, shape, or contour, persistent lumps or thickening in the breast or underarm, and discharge from the nipple, which may be blood-stained or clear. Early detection significantly improves treatment outcomes. Various imaging techniques are available for screening and diagnosing breast cancer, with mammography, ultrasound, and thermography being the most prevalent. Mammography, which uses X-rays, is the gold standard for early detection, while magnetic resonance imaging (MRI) is employed for high-risk individuals. Physical examinations, such as clinical breast exams performed by healthcare professionals and self-examinations, also play a vital role in early detection. Women's awareness of changes in their breasts, such as alterations in size, lumps, or pain, is essential in prompting timely medical consultation.

In this work, we present a Transformer-based Tiered-Stacking (TT-Stack) ensemble framework for mammogram-based breast cancer classification that will systematically combine seven lightweight vision transformer architectures (RepViT, DaViT, EfficientViT, MobileViT, FasterViT, MViT, and PVT v2) that each have properties for grayscale medical imaging. These proposed models have several important contributions with regard to:

- Proposing a unique two-tier meta-learning ensemble that takes each of the base-model logits concatenated into a 14-dimensional feature vector, then refines that with logistic regression, while taking advantage of differences in architectures (i.e. depthwise separable convolutions, dual attention, hierarchical multi-scale features for features) for better discriminative power.
- Introducing efficient grayscale-optimized transformer adaptation (in_chans=1) which can transfer learning from ROS-ready pre-trained weights, while retaining better parameter efficiency for clinically-ready use.
- Employing a stratified class-balanced training protocol which utilized upsampling-based balancing on the training set only to prevent leakage (and included a validation and test set), while implementing early stopping and ReduceLROnPlateau scheduling for eta.

- Benchmarking all models (engagement with transparency) in a multi-model framework (ROC-AUC, precision/recall, confusion-matrix) to establish performance baselines for transformer-based breast cancer detection.
- Establishing a modular pipeline ready for production (preprocessing, augmentation, reproducible training (SEED=42), and ensemble).

In contrast to the dominant methods for single-architecture models, the importance of TT-Stack frameworks for reducing a gap in medical AI is that lightweight transformers can be integrated into an ensemble, ultimately demonstrating that there can be improved generalization from fractional and complementary feature learning, while retaining computational fidelity to be practicable for world-ready screening workflows.

II. LITERATURE REVIEW

The detection of breast cancer has been thoroughly researched with various imaging modalities and machine learning techniques with the goal of improving the accuracy of diagnostics. In this section, we consolidate the most relevant investigations by organizing our sections around methodologies, imaging strategies, and comparisons of the advantages and disadvantages of studies. Sadoughi et al. [4], developed an extensive framework for detecting breast cancer that incorporated mammography, ultrasound, and thermography. They reported high accuracy of diagnosis using support vector machines (SVM) through the analysis of over 40 datasets. They rigorously investigated texture features, edge-based descriptors, and fuzzy techniques to compare the benefits and limitations of imaging modalities. In another study on mammographic microcalcifications, Prannoy and Saravanakumar [5], developed a computer-aided diagnosis (CAD) framework for diagnostic triage of the lesions between benign, normal and malignant. They use Principal Component Analysis (PCA) to reduce the dimensionality of the data they collected from DDSM database with approximately 3,000 samples, suggesting CAD use can be used to detect tumors responsible for the mammographic microcalcifications in cancer screening workflows. Neural networks have been developed and researched extensively in detection of breast cancer. Mekdy et al. [6] researched Artificial Neural Networks (ANNs), Backpropagation Neural Networks (BPNNs) and hybrid architectures with mammography, ultrasound, thermal imaging and MRI. They demonstrated that neural-network based models reduce false-positive and false negatives significantly, illustrating their flexibility and adaptability to complex imaging datasets.

Guzmán-Cabrera et al. [7] presented a CAD system specifically for digital mammography, incorporating texture segmentation and morphological operators. Their method is characterized by the combination of three methods: texture segmentation, morphology driven extraction of the suspicious region, and machine learning with entropy-based methods. Their framework combines these strategies with high accuracy and furthers the goal of totally automatic mammographic image analysis. Jasti et al. [8] presented a model for breast cancer classification utilizing both conventional machine learning and

deep learning. Their model combines image-processing steps of breast tissue analysis with conventional models (LS-SVM, K-Nearest Neighbors (KNN), Random Forest, and Naïve Bayes) and deep learning models (feature extraction with AlexNet and then CNN). Their multi-level pipeline generated high precision and revealed benefits of utilizing a combination of hand-crafted features and deep representations. Finally, Uswatun et al. [9] utilized the Watershed Transform Algorithm to detect breast cancer, reporting a diagnostic accuracy of 88.65% and an average segmentation error of 11.35% across 100 ultrasound images. Their findings show the important role of lesion segmentation in making classification reliable and that lesion segmentation and classification reporting is important for decreasing diagnostic error. In addition to breast cancer, Vision Transformers (ViTs) and hybrid CNN–Transformer models have been researched more broadly in related fields of medical imaging, and can offer additional methodological insights for our study. For example, Jahangir et al. [10] conducted an investigation into brain tumor classification with several CNNs and ViTs, focusing on their performance and providing metrics for discussion: precision, recall, and F1-score. Although the ViT model variants (L/32, L/16, B/32, B/16) reported perfect training statistics (i.e. 100% precision, recall, and F1-score), the CNNs were ultimately better at generalization, providing precision of roughly 98.233% on the test set, recall 98.271%, and F1-score 98.234%. It is worth noting that the authors also established several phases in their study such as establishing the process for training six CNN-based transfer learning models and four ViT variants in a uniform way, ultimately identifying the influence of deeper model capacity while indicating generalization as a key concept. Similarly, Chauhan et al. [11] created a model known as Patch-Based Vision Transformers (PBViT) for the detection of brain tumours, ultimately using them on the Figshare dataset. The outcome reported that the PBViT was better than the standard CNN architectures and for this group of patients the following metrics were achieved: accuracy 95.8%; precision 95.3%; recall 93.2; F1-score 92%. The study reported that the PBViT architecture included extra DenseNet blocks and custom CNN layers as part of the transformer model, which appears to allow a richer feature extraction process, while improving the representation of tumor boundary detection compared to previous works.

Simon and Briassouli [12] conducted a study comparing only Transformer-based networks for brain tumor classification and their performance against CNNs. Their ViT model performed with an accuracy of 96.5%, outpacing the CNN baseline of 89.78%. The authors employed data augmentation to address the class imbalance and improve generalization, which highlighted the benefits of ViTs in classifying complex medical images. Moreover, Asiri et al. [13] conducted a more systematic investigation of ViTs specifically focusing on the aspect of evaluation by fine-tuning five pre-trained models (R50-ViT-l16, ViT-l16, ViT-l32, ViT-b16, and ViT-b32) to perform targeted tasks in medical images. Performance was evaluated using metrics including precision, recall, F1-score,

accuracy, and confusion matrices. The authors aforementioned highlighted the ViT-b32 as performing with the best classification accuracy of 98.24%. It should also be noted that the authors fixed a number of hyperparameters (learning rate 0.0001, training batch sizes adapted to context, and ten epochs of training with Adam optimizer) which provided robust performance for the models they evaluated via their tuning of a number of hyperparameters. Tariq et al. [14] proposed a framework for multiclass brain tumor classification using deep learning based on EfficientNetV2 and ViT architectures. The EfficientNetV2 model achieved 95% accuracy, with a loss of 0.13, as well as 0.96 for F1-score, precision, and recall. The ViT model achieved 90% accuracy, with a loss of 0.30, as well as 0.89 for F1-score, precision and recall. Their ensemble approach, based on geometric mean, yielded an accuracy of 96% and outperformed the independent models. The study also did extensive data augmentation (rotation, flipping, scaling, cropping, and color adjustments) with a Kaggle MRI dataset. In addition to testing good predictive performance, they showed feasibility, with an average inference time of .35 seconds per image at inference, and 4.5 GB of GPU memory for inference and 12GB in training, using an NVIDIA RTX 2080. Guo and Fan [15] implemented a pre-trained ViT to classify multi-label lung cancer on histological slices using the LC25000 dataset, using both zero-shot and few-shot settings. Using a few-shot setting, they reported an accuracy of 99.87% at epoch 1, with peak performance at epoch 5. These results indicate the strength of data efficiency and transferability of the ViT.

Sun et al. [16] studied Swin Transformer models for lung cancer classification and segmentation. The Swin-B model achieved a top-1 classification accuracy of 82.26%, which outperformed ViT by 2.529%. Their pipeline segmenting an RGB lung CT image into non-overlapping patches for linear embedding and this was followed by a set of Swin Transformer blocks, which consisted of layers based on shifted windows, multi-head self-attention (MSA) layers, and multilayer perceptron (MLP) layers; each set of layers proceeded with the application of layer normalization and residual connections. While Swin-B served as the testing model for their project, only partial experiments were conducted for Swin-T and Swin-S due to limited hardware, which nonetheless emphasized the advantages of using hierarchical transformers. Durgam et al. [17], proposed the Cancer Nexus Synergy (CanNS) framework for cancer diagnosis, that included: a Swin Transformer-based unsupervised U-Net segmentation model (SwinNet), an Xception–LSTM GAN (XLG) for classification, and Devilish Levy Optimization (DevLO) for hyperparameter tuning. The CanNS framework demonstrated balance regarding computational cost and accuracy when evaluated on a Kaggle dataset and this stressed how segmented transformer models can be incorporated with advanced optimization under a single cancer-diagnosis pipeline. Chen et al. [18] developed an automated lung cancer detection framework that combines two approaches named CNN and Transformer. Specifically, the framework uses Mask R-CNN to segment lung cells and a

Swin Transformer to classify them. The proposed architecture yields accuracy results that surpass classical CNN architectures, including ResNet50, reaching a classification accuracy of 96.16%. Experiments were performed in Ubuntu 18.04.5 OS, using the programming language Python and a framework called PyTorch version 1.10.1, as well as an NVIDIA GeForce RTX 2080Ti GPU. The authors split the data sets into a train/test split of 70%/30% and used for training periods of 100 epochs, a batch size of 12, and learning rate decays at training epochs 30, 60, and 80. Akbari et al. [19] presented an approach using a ViT-based method for analyzing histopathological images, employing self-attention to extract salient features from histopathological images based on data sets from the LC25000 and IQ-OTH/NCCD. The approach's ViT to achieve accuracy results from 98.80% to 99.09%, outperforming a baseline using CNNs. The authors used the Adam optimizer and set a learning rate of 0.000001 for 50 epochs and with a batch size of 32 with experiments incorporating early stopping, model checkpointing, and a learning rate scheme. The authors used an extensive augmentation and preprocessing pipeline, implemented via image data generators to analyze histopathological images on a Windows 10 OS using the Python programming language and Anaconda. Ouamane et al. [20] conducted an ablation study detailing ViT architecture parameters, including patch size, image resolution embedding dimension, depth of transformer, number of attention heads, as well as MLP size. Their architecture was tested on the PlantVillage data set, reporting on the configuration that produced their optimal results achieving 99.77% accuracy for the machine learning classification architecture.

Carolin et al. [21] evaluated ViT architectures using the pre-trained L16 and L32 models for skin lesion classification and compared their performance against decision trees, KNN, CNNs, and a simpler ViT models. The accuracy of ViT-L32 reached 91.57% with a recall for melanoma classification at 58.54% while the ViT-L16 model achieved 92.79% accuracy with a melanoma recall of 56.10%. Their proposed method included an augmentation step followed by transfer learning and illustrates the potential of ViT to improve analysis of dermatological images. Koushik and Karthik [22] utilized fine-tuning of several pre-trained models for the detection of COVID-19 from chest x-rays, employing DenseNet, InceptionV3, WideResNet101 and ViT-B/32. They reported classification accuracy of 97.61%, precision of 95.34%, recall of 93.84%, and an F1 score of 94.58% when writing about all models initialized from ImageNet weights with the original classification heads replaced to match the task of COVID-19 detection. They used the RectifiedAdam optimizer with a ReduceLROnPlateau schedule, adding further evidence for the usefulness of a CNN-ViT hybrid approach to thoracic imaging. Finally, Gelan and Se-woon [23], validated their BUViTNet framework to two public breast ultrasound datasets (Mendeley and BUSI). On the Mendeley dataset, BUViTNet achieved AUC, MCC and Kappa scores of 1 ± 0 , while on BUSI it achieved an AUC of 0.968 ± 0.02 , an MCC of 0.961 ± 0.01 and Kappa of 0.959 ± 0.02 . BUViTNet outperformed ViT models

trained from scratch and ViT-CNN based transfer learning models which emphasizes the efficacy of transformer-based architectures in breast ultrasound image classification.

In all, these studies reveal a definitive trend in modern CAD systems for oncology that rely more and more on deep learning and, in particular, Transformer based architectures (ViT, Swin Transformer, and mixed) across modalities (mammography, ultrasound, MRI, CT, and histopathology). This body of literature presents both methodological reasoning and empirical motivation for the proposed Transformer based, multi-backbone, and stacking-ensemble framework for mammographic breast cancer detection.

III. BACKGROUND STUDY

Despite better survival statistics worldwide, breast cancer remains the second leading cause of cancer deaths, and prognosis heavily relies on the timing of diagnosis. This is why imaging has become a major factor in screening and diagnosis. Traditional imaging modalities (mammography, ultrasound, and thermography) alongside newer modalities (breast MRI in particular and especially for higher risk groups within the population) have been steadily evolving. Mammography is viewed as the gold standard for any population-based screening, particularly if coupled with a clinical or self-examination, as the imaging modality can detect subtle abnormality prior to symptom appearance. Deep learning has been thoroughly investigated as assistive to radiologists, when interpreting these images. In particular, CNNs that can be trained to appreciate local texture and edge structures, and have shown promise in a number of breast-imaging studies. However, due to the stationary receptive fields (RF), focused processing of local patterns have also limited CNNs capacity to model long-range contextual dependencies important for both the characterization of subtle lesions and breast-wide context to ensure a comprehensive interpretation of diagnosis. Vision transformers (ViTs) were developed first for natural language processing, but then refined in the image domain when examining an image as a sequence of patches computed in a self-attention fashion (and allow for global context modeling and flexibility in receptive field, while also allowing scalability).

More recent works have introduced several different kinds of transformers aimed at efficiency and/or deployment limitations. RepViT [24] modifies MobileNet style CNNs with token/channel attention decoupling and structural reparametrization, especially obtaining very high ImageNet performance under strict mobile latency restrictions, still attractive for on-device inferences. EfficientViT [26] tackles the memory bottlenecks on attention with a sandwich layout and cascaded group attention, balancing memory restricted operation with minimal cost of accuracy. MobileViT [27] employs hybrid blocks that encode local (by convolutions) and global information (with light-weight transformers) resulting in very competitive performance across image classification, detection and segmentation all with significantly lower parameters and capacity for real-time processing on edge devices. FasterViT [28] extends the speed-accuracy trade-off even further with a

hierarchical attention mechanism leveraging learning carrier tokens to propagate global information across windows at almost linear complexity with respect to image resolution. In contrast to the lightweight families discussed earlier, several architectures have developed highcapacity design choices to better capture richer spatial and semantic structure. DaViT [25] modifies the dual attention in spatial windows and channel groups, respectively modeling the local detail and global channel independence. Multiscale Vision Transformers (MViT) [29] implement a hierarchical architecture with decreasing spatial size and increasing channel depth, using effective multiscale feature pyramids from CNNs to process dense spatiotemporal signals. PVT-v2 [30] facilitates linear spatial-reduction attention, overlapping patch embeddings, and convolutional feed-forward, and introduces a versatile full-scale pyramid backbone applying to high-resolution dense prediction tasks.

In total, our seven models, RepViT, DaViT, EfficientViT, MobileViT, FasterViT, MViT and PVT-v2, encompass a wide range of design decisions for its attention mechanisms and its multiscale representations for various computational costs. They are very effective in the large-scale natural image and other downstream vision tasks, and therefore are considered candidate models for the medical imaging field. We therefore evaluate their performance for mammography-based breast cancer diagnosis when compared under a common training and testing protocol for insight to how trendy transformer architectures are expected to map to clinical screening products.

IV. METHODOLOGY

Our suggested framework defines mammogram analysis as binary image classification, where each grayscale mammogram is classified as either Cancer or Non-Cancer, using the “Mammogram Mastery: A Robust Dataset for Breast Cancer Detection and Medical Education.” All images are loaded as single-channel 8-bit mammograms and converted to PIL format. To create an unbiased evaluation, the dataset is split into disjoint training and validation sets in an 80/20 stratified split, preserving the overall class distributions and proportions in both splits and overall split of class distributions. Given that screening cohorts are naturally imbalanced, and consist mostly of non-cancer cases, only the training split is class balanced by upsampling the minority class with replacement, until each class has an equal number of samples, and the validation split is untouched, so that they would reflect realistic prevalence.

Prior to feeding the models, all images are pre-processed through a uniform pipeline. Each mammogram was resized to 224×224 pixels, in order to meet the input requirement of the chosen backbones and represent a reasonable compromise among different dimensions of spatial detail and computational load. A lightweight augmentation approach was used while training the models, consisting of random horizontal flips and small random rotations $\pm 5^\circ$, to generate reasonable acquisition variability without distorting lesion morphology. The augmented images were converted to tensors and subsequently normalization was completed with mean

$= 0.5$ and $\text{std} = 0.5$, effectively scaling the intensities to approximately $[-1, 1]$. The same steps for resizing and normalization were completed with validation images, without the random transformations. Batches were generated using PyTorch DataLoaders (batch size 64) with shuffling to train and validate. The backbone evaluation stage investigates a wide variety of compact and efficient vision transformers. The studied sample is seven, as follows: RepViT (repvit_m1_0), DaViT (davit_tiny), EfficientViT (efficientvit_b1), MobileViT (mobilevit_xs), FasterViT-0 (faster_vit_0_224), MViT v2 Tiny (mvitv2_tiny) and PVT v2 B0 (pvt_v2_b0). All models are initialized with weights pretrained on ImageNet and adapted to the context for mammography by changing the number of input channels to 1, and, replacing the original classification heads with fully connected heads set to 2 output neurons, 1 for the Cancer class and 1 for the Non-Cancer class. For FasterViT, the official implementation was run as a 1000-headed feature extractor, which was then plugged into a new linear head that mapped the 1000 logits to the 2 target classes. Thus, for each input image, every backbone produces a two-headed logit vector that yields unnormalized evidence for both Cancer and Non-Cancer.

To provide a fair comparison, all backbones are fine-tuned in an end-to-end manner across the same training protocol. Training is done in PyTorch with the AdamW optimizer with $1e-4$ as the starting learning rate and weight decay, while the optimization objective is cross-entropy loss. The validation loss is monitored through a ReduceLROnPlateau scheduler which terminates the learning rate when there is no decrease in validation loss for three epochs by halving the initial learning rate. Each model is trained for a maximum of 30 epochs while global seeds are fixed to guarantee reproducibility across both NumPy and PyTorch (including CUDA). After each epoch, loss and accuracy are computed on both the training and validation sets. The lowest validation loss checkpoint is kept as the final version of the backbone, which serves as an implicit early stopping rule with an implementation of reloading those best weights prior to any downstream evaluation or ensembling. For the best checkpoint, the model generates logits for every validation sample, which are converted to predicted labels via argmax across the two classes. Next, the framework evaluates the model’s predictions to compute accuracy, precision, recall, F1-score and a full classification report for both Cancer and Non-Cancer. In order to evaluate discriminative ability at all decision thresholds, softmax probabilities for the positive class are used to produce receiver operating characteristic (ROC) curves and compute ROC area under the curve (ROC-AUC). Confusion matrices are also generated to visualize the distribution of true positives, true negatives, false positives and false negatives. All metrics are collated in a comparison table and the ROC curves and confusion-matrix heatmaps are saved as individual figures for further evaluation.

In addition to these individual backbones, the paper presents a two-tier stacking ensemble, called TT-Stack, in which the heterogeneous backbones complement each other’s performance. The first layer consists of all seven fine-tuned back-

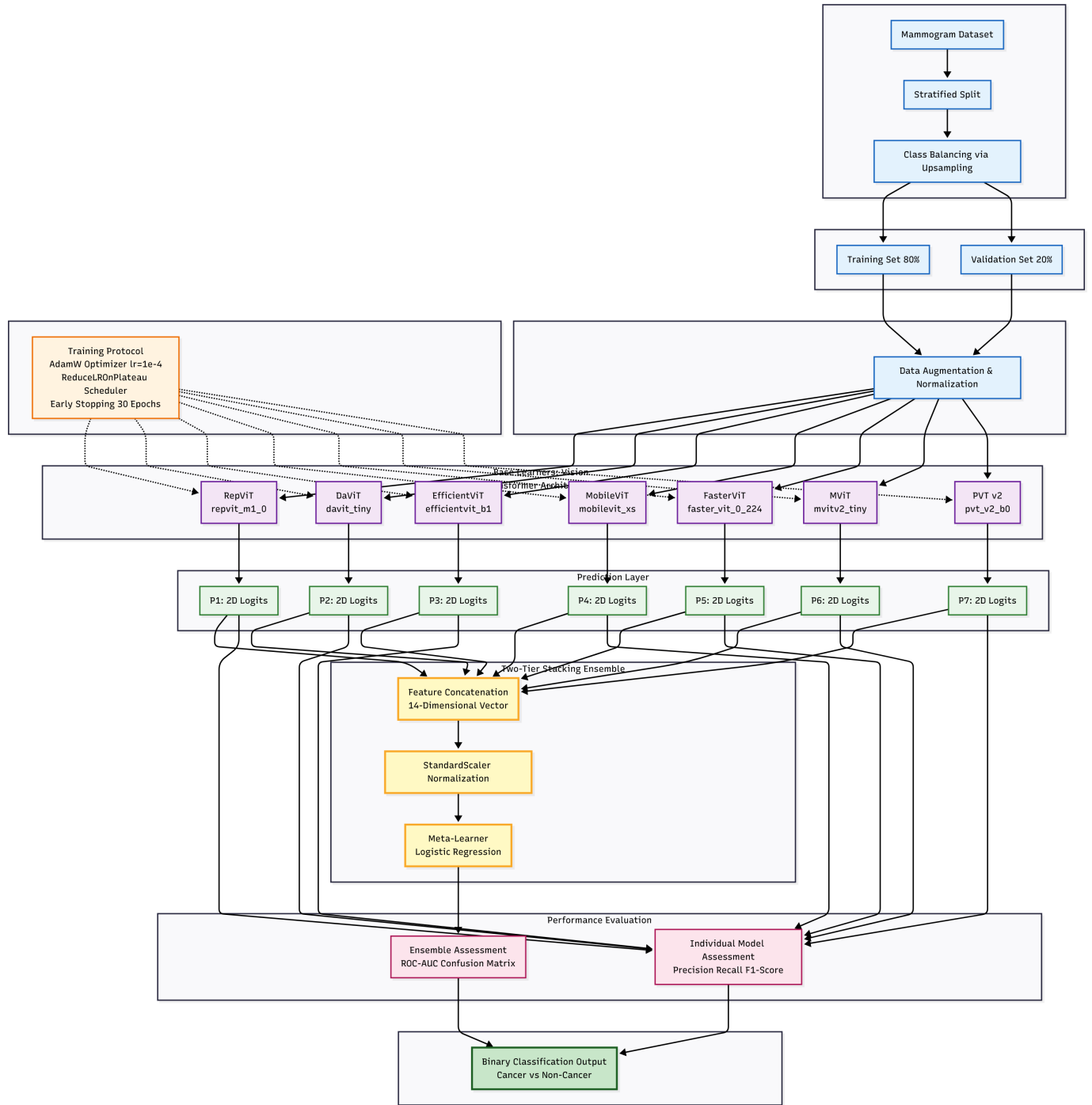


Fig. 1: Overall architecture of the proposed TT-Stack mammogram classification pipeline, including data preprocessing, backbone fine-tuning, and stacking ensemble.

bones acting as frozen base learners. For each image in the balanced training loader and in the validation loader, each backbone runs in evaluation mode to output its associated two-dimensional logit vector. The logits produced by all the backbones are concatenated (across backbones) into a single $2K$ -dimensional feature vector (where K is the number of backbones; $K = 7$ for the full configuration, which indicates that there are 14 features produced for each image). This process is repeated over all batches, producing a meta-training feature matrix and a meta-validation feature matrix, both of which align to the original ground-truth labels. The second tier of TT-Stack is comprised of a logistic regression meta-classifier applied to the concatenated logits. The meta-learner uses a scikit-learn pipeline and consists of a StandardScaler to normalize each feature dimension and a logistic regression classifier with `class_weight="balanced"`, a maximum of 500 iterations, and parallel optimization (`n_jobs=-1`). The model is trained on the meta-training features and labels only; the meta-validation set is not seen during meta-training. At inference time, TT-Stack first forwards an image through all frozen backbones to retrieve their logits, then concatenates the logits, homogenizes the resulting vector prior to applying the learned logistic regression weights to predict the final probability of cancer/non-cancer/normal. The evaluation of the performance of the ensemble is established with the meta-validation set using the same metrics as for the individual model evaluations: accuracy, precision, recall, F1-score, ROC-AUC, and the confusion matrix which illustrates how the proposed stacking strategy is shown to aggregate the diverse transformer predictions into one collective decision-making system to detect breast cancer from mammograms.

V. RESULTS AND ANALYSIS

The experimental results in Table I show that all vision-transformer models under investigation approximate the training distribution very efficiently, as manifested by close to 100% train accuracy and loss down to small values across almost of all models, but importantly differ in how much such efficiency generalizes to unseen data. The most applied generalization is reached by EfficientViT and PVT v2, which are on a very clear top level. Both models have highest F1-scores = 0.9796 and best validation accuracies (EfficientViT, PVT v2: 0.9933), along with lowest validation losses (EfficientViT, PVT v2: 0.0119, 0.0190). Their train-validation accuracy spreads are the lowest of the cohort (approximately 0.67 percent points), which implies that those architectures learn the data with great proficiency, in absence of severe overfitting. This is supported by the ROC_AUC of 1.000, indicating an almost perfect class separability and an extremely robust ranking of positive against negative ones.

A second competitive layer is constructed by DaViT and MViT. Both models reach precision and recall of 0.96, so F1-scores of 0.96 plus validation accuracy of 0.9866. Despite their validation losses (0.0471 and 0.0677, respectively) being larger than EfficientViT's and PVT v2's, they prove to be highly discriminative as well, with ROC_AUCs over 0.999. (Note:

The modestly larger train-validation gaps (approximately 1.34 p.p.) indicate some tendency to overfit in comparison with the highest-scoring model, but not one that would render such models of little practical use.) In scenarios with diminishing returns in validation accuracy where the proposed reductions are tolerable, these architectures continue to be compelling choices if other system level considerations (e.g., deployment constraints discussed elsewhere in this paper) are more positive toward them. RepViT and FasterViT are just in the middle of performance among various designs. RepViT reaches highest precision (1.000) but the lowest recall (0.88) in the set, it achieves an F1-score of 0.9362 and a validation accuracy of 0.9799. This tendency reflects a threshold that is conservative in nature, one that minimizes the number of false positives at the expense of overlooking more true positives. FasterViT conversely shows an intermediary precision-recall trade-off (0.9583 and 0.92), resulting in a slighter F1-score of 0.9388, together with the smallest validation loss (0.1186) translated into less stable generalization as compared to the top performing variants due primarily to larger train-validation accuracy gap (2.01 percentage points). However, both the two models with some pruned layers still have ROC_AUC more than 0.995, which indicates that they are qualified for strong ranking even their operating point on the ROC is not as competitive as EfficientViT, PVT v2, DaViT or MViT.

Overall, MobileViT is consistently inferior to more the other architectures in terms of most metrics. In the second group, its precision is lower at 0.80 and a high recall rate of 0.96, but it unbalances the precision-recall tradeoff which is reflected as an F1-score of 0.8727 in these terms. The model exhibits the smallest train-validation gap (4.40 percentage points) which show an enhanced overfitting effect as compared to others, accompanied by the lowest validation accuracy (0.9530) and highest validation loss (0.1641). The ROC_AUC of 0.9868, albeit a very high figure in the absolute sense, is certainly lower when compared with the near perfect AUCs achieved by the other contenders. In general, the comparison analysis demonstrates that all transformer-based models benefit from excellent representation learning; nonetheless, Asteroid (62.8 1.0% in WER%) presents the optimum trade-off between accuracy and robustness; CovidAID correctly recognizes nine classes with an average harmonic recall of 97% on Imbalanced any other efficient model: Two EfficientViT and PVT v2 excel as effective alternative to DaViT models according these three criteria (standard deviation).



Fig. 2: After analyzing images from both cancerous and non-cancerous cases.

TABLE I: ANALYZING PERFORMANCE MEASURES IN COMPARISON TO OTHER TECHNIQUES

Model	Precision	Recall	F1-Score	Training Accuracy	Training Loss	Validation Accuracy	Validation Loss	ROC_AUC
RepViT	1.000000	0.88	0.936170	0.997984	0.008955	0.979866	0.053015	0.996129
DaViT	0.960000	0.96	0.960000	1.000000	0.000349	0.986577	0.047081	0.999677
EfficientViT	1.000000	0.96	0.979592	1.000000	0.000318	0.993289	0.011955	1.000
MobileViT	0.800000	0.96	0.872727	0.996976	0.014560	0.953020	0.164069	0.986774
FasterViT	0.958333	0.92	0.938776	1.000000	0.002385	0.979866	0.118583	0.995484
MViT	0.960000	0.96	0.960000	1.000000	0.000084	0.986577	0.067721	0.999355
PVT v2	1.000000	0.96	0.979592	1.000000	0.000037	0.993289	0.019008	1.000

In Figure 2, we can show the images that we get after training our models which is able to detect Cancer and Non-cancer images.

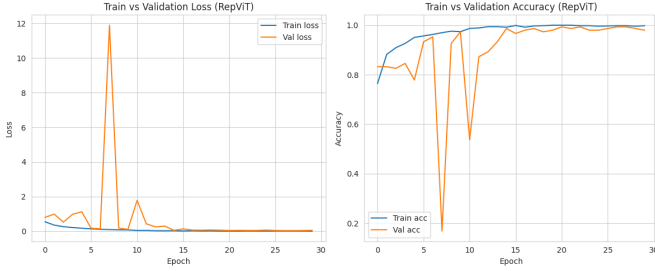


Fig. 3: Training and Validation Accuracy and Loss Curves for RepViT.

The RepViT learning curves in figure 3 indicates efficiency and some “initially” poor generalization. The training error declines nicely to zero and it appears that the model is overfitted to the data since the train accuracy goes from about 0.78 to close to 1.0. Nevertheless, the validation curves show a couple of earlier spikes in loss and drops in accuracy that suggest only potential transient susceptibility to optimization dynamics or data variability (in contrast to sustained overfitting). The validation loss plateaus at a low value after around the 12th epoch and the validation accuracy lingers high in the range 0.97–0.99, which validates our diving behavior during training. This result also confirms that RepViT finally converges into a well-generalized solution although such convergence progress was not visible during the initial epochs of training.

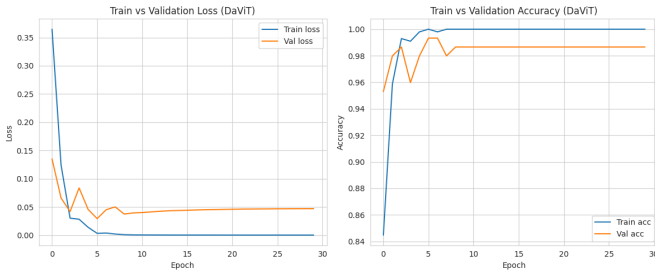


Fig. 4: Training and Validation Accuracy and Loss Curves for DaViT.

The DaViT learning curves in figure 4 demonstrate fast and robust convergence with a small train–validation gap. The

training loss falls precipitously from 0.36 to nearly zeros in the first 5–6 epochs, and the training accuracy increases dramatically from 0.85 to almost 1.0, suggesting that the model swiftly learns to fit on the training distribution. Validation loss has its descent, followed by a plateau at low value (0.045), while the validation accuracy reaches approximately 0.99 and stays a bit below training counterpart. This behavior shows good generalization with marginal overfitting, validating DaViT as a well-calibrated backbone for this task.

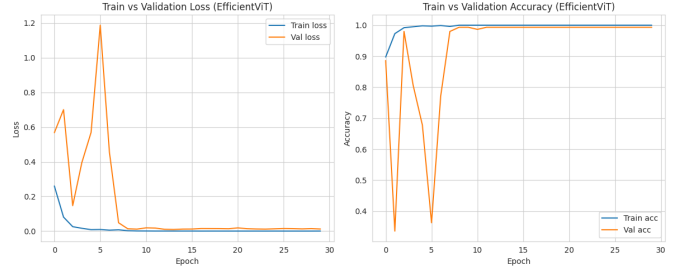


Fig. 5: Training and Validation Accuracy and Loss Curves for EfficientViT .

Figure 5: EfficientViT learning-curves show a fast convergence phase with short instable start on the validation set. The training loss starts with a very high value approximately 0.26 and decreases rapidly to nearly 0 throughout the first few epochs, then continues being small enough, in line with the fast fitting of the model to the training data. On the other hand, the validation loss first fluctuates with a peak around 5 epochs introduced by sharp valleys in the validation accuracy, indicating temporary sensitivity to optimization dynamics. However around epoch 7 validation loss stabilizes at a very low level and closely follows the training curve while validation accuracy rises to approximately 0.99. The fact that the small and stable train–validation gap is such an optimization canary indicates that, after a period of volatility, EfficientViT ultimately generalizes extremely well on this task with mild reliability stronger than DaViT.

The MobileViT learning curves presented in figure 6 exhibit slower and more unstable convergence than the stronger backbones. The training loss continuously decreases at a smooth pace to reach a level close to zero whereas the training accuracy increases from 0.86 to approximately 0.99, indicating that the model learns quite well from input data inferred at image resolution. But as compared to the smooth descending pattern

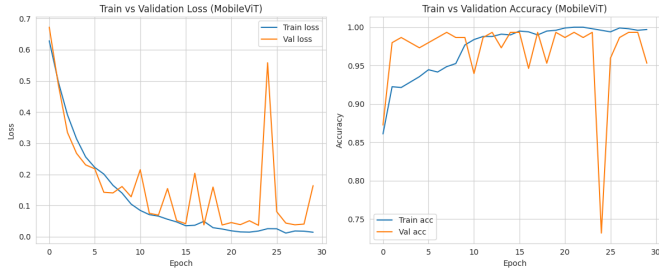


Fig. 6: Training and Validation Accuracy and Loss Curves for MobileViT.

in the training loss, there are several spikes in validation loss, notably during epochs 22–24, and validation accuracy is swinging back and forth sharply with a sudden drop near epoch 24 before partly recovery. This disconnect between smooth training but volatile validation behavior, and consistently worse validation loss, suggest weaker generalization and sensitivity to data variation or optimization noise. In general, MobileViT achieves similar peak validation accuracy as other ViT based models, but with considerably worse reliability and stability.

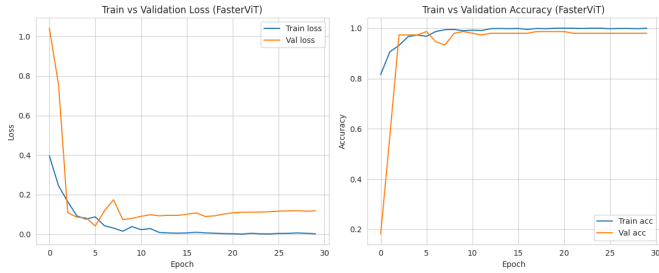


Fig. 7: Training and Validation Accuracy and Loss Curves for FasterViT.

Training curves of FasterViT in fig 7 also manifest quick and relatively convergent with little gap between train, validation performance. The training loss decreases rapidly from approximately 0.40 to almost zero within the first epoch and then saturates to a very small value, and the training accuracy increases from 0.81 to 1.0, revealing an extremely good fit to the training data set. The validation loss also decreases but flattens out on a higher plateau (0.11–0.13) and the validation accuracy increases sharply from an initial low value to approximately 0.97–0.98, below the training curve (Figure 1). This small discrepancy between training and validation is consistent throughout, indicating mild overfitting, but overall we see strong generalisation with much less variance than MobileViT and only slightly lower stability to the best performing EfficientViT and PVT v2 backbones.

The MViT learning curves in figure 8 show saturation for the validation performance, as well as a generalization gap that never completely disappears. The training loss drops sharply from approximately 0.36 to virtually zero in the first 4 epochs, and the training accuracy increases from 0.85 to

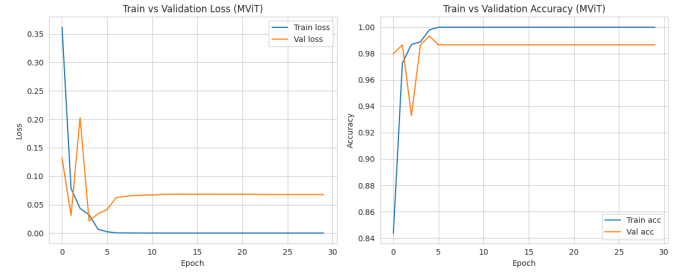


Fig. 8: Training and Validation Accuracy and Loss Curves for MViT.

plateau at its maximum value of 1.0, indicating that the model rapidly overfits on the training data distribution. Validation loss shows some early transients including a peak around epoch 2–3 followed by a shallow plateau near 0.06, and validation accuracy increases to 0.985 just under the saturated training curve. Both relative to EfficientViT or PVT v2 and MobileViT, where this was not the case, this stable behavior is the likely cause for a slightly more conservative model structure overall (with full dataset train–validation gap of still $\epsilon^* \approx 15\%$ instead of less than $\epsilon/4$), despite dominant mean performance.

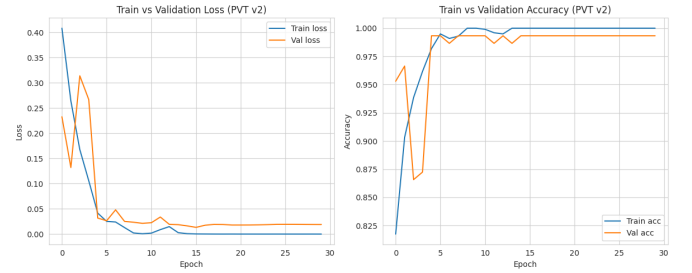


Fig. 9: Training and Validation Accuracy and Loss Curves for PVT v2.

The PVT v2 learning curves in figure 9 demonstrate rapid and stable convergence with excellent alignment between training and validation performance. The training loss quickly decreases from 0.41 to almost 0 within the first 5–6 epochs: and the training accuracy increases starting at 0.8, and reaching 1.0 after less than half of the cycles, meaning that the model captures extremely well even on the training data. The validation loss decreases initially erratically, but then immediately takes the same path down as training while converging to a very low value (0.02), and similarly validation accuracy jumps at an early stage of learning from 0.95 to approximately 0.99 almost parallelly with the training curve only with small lag. These low, well-aligned losses combined with the train–validation accuracy profile that is also nearly identical reveals PVT v2 to be one of the most reliably generalized and well-calibrated models in this cohort, when compared across backbones.

Overall, it is evident from the learning curves presented in Figures 3–9 that all seven architectures have shown similarly high training performance in their consistent training accuracy,

but the degree of convergence stability and resulting generalization differed in meaningful ways. PVT v2 and EfficientViT created the strongest grouping as they had very (none, incomparable) loss measure at training accuracy, with both models having excellent loss minimization, yet also training accuracy close to perfect after relatively few epochs. Validation losses were low while validation accuracy quickly began to plateau around 0.99 for both models, with only a slight, unproblematic gap between training and validation. Next, DaViT and MViT behaved similarly to PVT v2 and EfficientViT, converging quickly to mid to high 0.98–0.99 validation accuracy, and with training accuracy saturating to 1.0 concern. However, DaViT and MViT have slightly higher asymptotic validation losses (only a range of <0.045 to 0.06), with a more sizeable gap to the training curves than PVT v2 and EfficientViT, indicating mild overfitting and less calibrating strength than the superior models. Lastly, RepViT provided a similar, but higher final validation accuracy (0.97 to 0.99), and demonstrated liquid curves as portrayed by two large early spikes in and around epoch 2–4, demonstrating instability before converging with an up trend on both curves in around the 12 epoch mark to begin reaching satisfactory or promising generalized levels. FasterViT had soft and angular curves converging towards similar, but slower validation training accuracy as between 0.97 and 0.98, yielded loss elements plateauing however at relatively higher levels of loss (0.11 to 0.13), evidencing on validation centering and modelling towards slow, and mild gap towards potential but persistent generalization gap. In comparison, it is evident that MobileViT is the most unstable of the group. While it has a smooth decrease in training loss and training accuracy approaches 0.99, the validation curves clearly show repeated spikes in loss and oscillations in accuracy, including a complete collapse in performance around epoch 24 and partial recovery. A divergence between smoothly improving metrics in training and volatile validation metrics suggests MobileViT is more sensitive to data variability, or optimizing noise, which would explain the less robust and reliable generalization when judging performance compared to the other ViT-based models. Overall, the comparison of the curves assigns PVT v2 and EfficientViT as the best behaved and most reliable backbones and DaViT, MViT, RepViT, and FasterViT as strong but slightly more overfit or transiently unstable, with MobileViT as the most fragile even if the contemporaneous accuracy was competitive in the peak epoch.

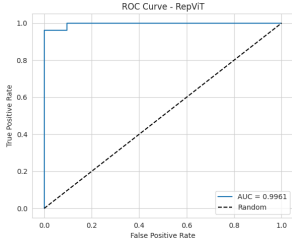


Fig. 10: ROC-AUC Curve for RepViT.

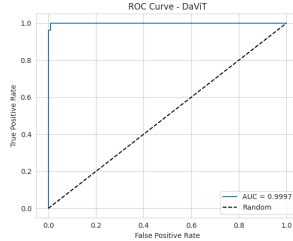


Fig. 11: ROC-AUC Curve for DaViT.

The ROC curve in Figure 10 for RepViT indicates that it provides near-perfect discriminative ability on the test data. The curve rises steeply toward the upper-left of the graph. It achieves very high true-positive rates with extremely low false-positive rates, and it remains very well above the diagonal random-chance line throughout all thresholds. The AUC of 0.9961 indicates that RepViT performs almost perfectly in ranking instances positive above instances negative, demonstrating that the class manifests itself in this classification task reliably. The ROC curve in Figure 11 for DaViT indicates the same virtual perfection in discrimination. The curve rises almost vertically from the origin toward the upper-left of the graph; by the time the curve achieves high true-positive rates, the false-positive rates are practically zero, and the curve remains far from the random-chance line. The resulting AUC of 0.9997 indicates that DaViT is very effective at distinguishing positive from negative samples, demonstrating excellent robustness on the test data. The ROC curve in Figure 12 for EfficientViT reflects ideal classification behaviour. The curve rises almost straight up from the origin to a true-positive rate of 1.0 at nearly-zero false-positive rates, and then runs horizontally along the upper axis, as far as possible from the diagonal reference line. The resulting AUC of 1.0000 indicates perfect separability.

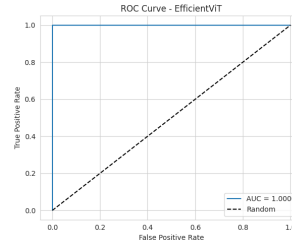


Fig. 12: ROC-AUC Curve for EfficientViT.

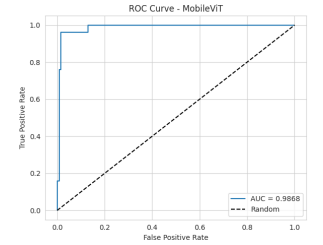


Fig. 13: ROC-AUC Curve for MobileViT.

The ROC curve for MobileViT which is shown in Figure 13 shows strong, although somewhat weaker, discriminative capacity compared to the best backbones. The ROC curve was well above the random-chance diagonal and achieved high true-positive rates for low false-positive rates, suggesting good separation of classes at thresholds. The ROC curve trajectory, however, was not as steep and not as clustered toward the upper-left corner compared to the ROC curves from DaViT, EfficientViT or PVT v2. With a AUC of 0.9868, MobileViT still has great separability capacities, however, it has slightly lower ranking capacity and reliability than the top models previously discussed. The ROC curve for FasterViT which is shown in Figure 14 is an excellent performing ROC curve. The ROC curve demonstrates a quickly upward trajectory relative to the upper-left corner while sustaining high true-positive rates for very low false-positive rates, while also being far above the random diagonal. The AUC ensures that FasterViT is extremely close to perfectly ordering positive and negative samples, and for this reason, the performance was similar to the top architectures. The ROC curve for MViT, shown

in Figure 15, also indicates nearly perfect discrimination. The curve rises almost vertically along the y-axis to a true-positive rate close to 1.0, at a very low false-positive rate, and subsequently tracks the upper boundary, lying well above the random baseline at all thresholds. The resulting AUC of 0.9994 demonstrates that MViT ranks positive examples above negatives very well and confirms its excellent robustness on the test set. The ROC curve for PVT v2 shown in Figure 16 indicates ideal behaviour, similar to EfficientViT. The curve rises almost vertically from the origin to a true-positive rate of 1.0 at effectively 0 false-positive rate and then maintains along the upper axis, maximally separated from the diagonal chance line over the full threshold range. The AUC of 1.0000 demonstrates perfect separability between positive and negative cases indicating that PVT v2 ranks class membership totally without error.

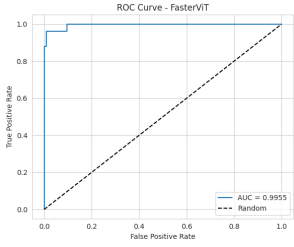


Fig. 14: ROC-AUC Curve for FasterViT.

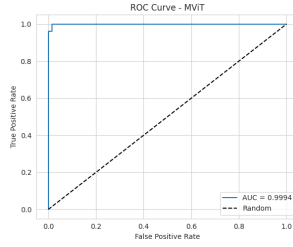


Fig. 15: ROC-AUC Curve for MViT.

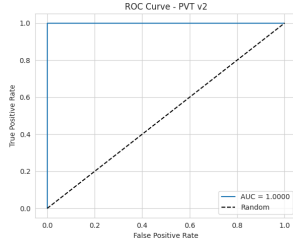


Fig. 16: ROC-AUC Curve for PVT v2.

Considering all of the ROC-AUC profiles, these results indicate that all seven architectures have excellent discriminatory ability ($AUC > 0.98$, several models are very close to a theoretical ideal). EfficientViT and PVT v2 achieve perfect ranking and, with an AUC of 1.0000, they enter the top tier of performance; MViT and DaViT show near perfection, with AUCs of 0.9994 and 0.9997, respectively. For RepViT and FasterViT, AUCs above 0.995 are also indicative of an excellent performance at only a small decrease in robustness. MobileViT exhibits an excellent AUC of 0.9868, although it is a slight decrease compared to the others, which is consistent with the more variable validation behaviour that we identified in the learning curves. In summary, the ROC profiles align with the training-validation findings, which suggest that the ViT variants provide very dependable discrimination, with EfficientViT and PVT v2 emerging as the most dependable architectures across all ViTs in this measure of threshold-

independent performance.

When studies in the literature are examined, besides the accuracy measurement metric, precision (Prec), sensitivity (Recall), and F1 score (F1) metrics were observed to be used. These values can be calculated in matrix form using the confusion matrix. The true positive values (TP), true negative (TN), false positive (FP) and false negative (FN) can be calculated in the confusion matrices of the classification results. Table II shows the components of the confusion matrix

TABLE II: Confusion matrix.

Actual Value	Predicted Value	
	Positive	Negative
Positive	True Positive (TP)	False Negative (FN)
Negative	False Positive (FP)	True Negative (TN)

$$\text{Accuracy} = \frac{TP + TN}{TP + FP + FN + TN}$$

$$\text{Precision} = \frac{TP}{TP + FP}$$

$$\text{Recall} = \frac{TP}{TP + FN}$$

$$\text{F1-Score} = \frac{2 \times \text{Precision} \times \text{Recall}}{\text{Precision} + \text{Recall}}$$

A confusion matrix is a table that is often used to numerically determine the performance of a classification method on a test dataset where the actual values are known. The results of the confusion matrix on the data sets we used in the study are as follows:

- TP (True Positive): It means cancer.
- FP (False Positive): It means non-cancer cases as cancer.
- TN (True Negative): It means non-cancer.
- FN (False Negative): It means cancer case as non-cancer.

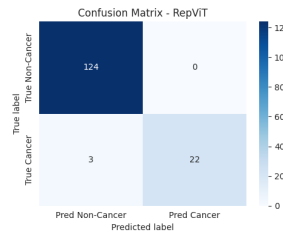


Fig. 17: Confusion Matrix of RepViT.

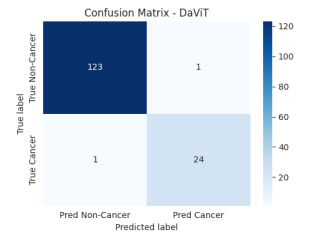


Fig. 18: Confusion Matrix of DaViT.

The confusion matrix for RepViT, shown in figure 17, demonstrates that the model identifies all 124 non-cancer cases as true negatives, as well as 22 out of 25 cancer cases as true positives, with no false positives and 3 false negatives. This results in a very high specificity (when a non-cancer case is never incorrectly identified as having cancer) at the cost of just a few missed cancer cases, which represents a small decrease in sensitivity. In the confusion matrix for DaViT, shown in figure 18, we see 123 true negatives and 24 true positives, with

just 1 false positive and 1 false negative. This means DaViT is missing one additional case misclassification out of the non-cancer cases compared to RepViT, and it has recovered two additional cancer cases. Thus, compared to RepViT, DaViT has a better balance in its low distance trade-off between sensitivity and specificity, which is preferred in a screening case like this. The EfficientViT confusion matrix, shown in figure 19, details 124 true negatives and 24 true positives, with 0 false and only 1 false negative case. This outcome represents near-perfect performance in both classes: there are no healthy subjects identified as having cancer and there was only one case of a missed cancer, providing high specificity and maximal sensitivity at the same time.

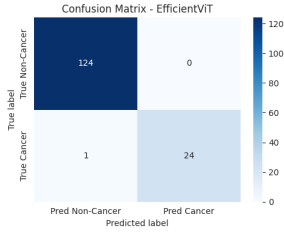


Fig. 19: Confusion Matrix of EfficientViT.

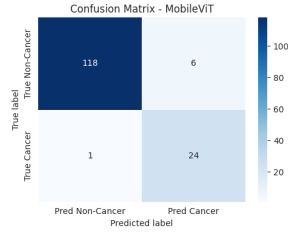


Fig. 20: Confusion Matrix of MobileViT.

For MobileViT, the matrix of figure 20 lists 118 true negatives and 24 true positives, as well as 6 false positives and 1 false negative. While cancer detection remains good, the increased number of false positives indicates that a larger proportion of cases that do not have cancer are predicted to have it, resulting in additional unnecessary follow-up, with no increase in sensitivity compared to DaViT, MViT, or PVT v2. Figure 22 shows the confusion matrix for FasterViT, with the outcome of 123 true negatives (TNs) and 23 true positives (TPs), and 1 false positive (FP) and 2 false negatives (FNs). Compared to DaViT, this model maintains a similarly low rate of first time false positives, but does miss 1 additional cancer case, so there is a slight drop in sensitivity but still a good specificity. For MViT, figure 22 shows a confusion matrix of 123 TNs and 24 TPs, but with only 1 FP and 1 FN. This means the profile for MViT is almost identical to that of DaViT, with very few false positives and only 1 missed malignancy, and so the performance is also well-balanced at an operating point of very few overdiagnoses and very few underdiagnoses. Finally, the PVT v2 confusion matrix of figure 23 shows a total of 124 TNs and 24 TPs, but with 0 FPs and 1 FN. Similar to EfficientViT, this version avoids falsely labelling healthy patients as cancer, but missed a total of only 1 malignancy, showing very high specificity.

In comparison, all the transformer-based backbones have good discrimination, but their error profiles show meaningful differences in clinical trade-offs. EfficientViT and PVT v2 stand out as the most conservative and accurate. They both had zero false positive errors and one false negative error, which is appealing when minimizing unnecessary follow-up is critical. DaViT and MViT are somewhat more permissive, but

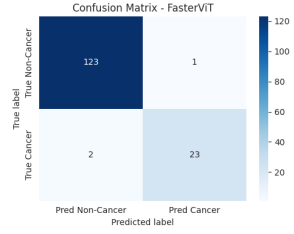


Fig. 21: Confusion Matrix of FasterViT.

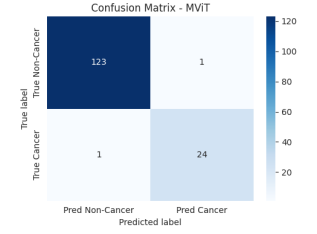


Fig. 22: Confusion Matrix of MViT.

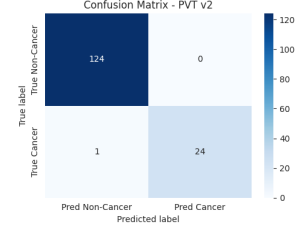


Fig. 23: Confusion Matrix of PVT v2.

still provide the same level of robustness, having one each of both types of errors. RepViT had perfect specificity, but three missed cancers; FasterViT had two missed cancers and one false positive; and MobileViT is the weakest by far with six false positives, despite comparable detection of cancer to most the other methods. Overall, the confusion matrices confirm the ROC and accuracy findings, indicating that EfficientViT and PVT v2, and followed by DaViT and MViT, are the most clinically credible approaches to breast cancer classification in this cohort.

TABLE III: TT-Stack Ensemble Validation Metrics

Propose Ensemble	Accuracy	Precision	Recall	F1-Score	ROC-AUC
TT-Stack	0.9933	1.0000	0.9600	0.9796	0.9997

The results in Table I show that each of the backbones achieves strong validation performance, but there are differences in how they trade precision, recall, and robustness. For example, RepViT and MobileViT appear more imbalanced (RepViT has low recall because it ranks some of higher severity observations low, while MobileViT has higher loss in validation). However, the best single model EfficientViT and PVT v2 achieved the highest validation accuracy (0.9933), precision (1.0000), recall (0.96), F1-score approximately 0.9796, and ROC-AUC of 1.0. DaViT and MViT perform slightly lower in F1 and ROC-AUC, while FasterViT is somewhat between both extremes. Overall, Table I indicates that no one backbone is best at all aspects of performance and stability; each of the models has small differences in either recall, specificity, and loss behaviour, therefore any of the backbones would be trusted with similar hesitancy. In response to the specific findings, we introduce the TT-Stack model in Table

III, to capture and reconcile the underlying complementary strengths of these backbones, and to achieve the effect of removing the underlying weaknesses. Quantitatively, TT-Stack achieved equivalent performance to the best single models on the headline metrics—accuracy of 0.9933, precision of 1.0000, recall of 0.9600, and F1-score of 0.9796—while achieving a ROC-AUC of 0.9997 that represents an effective AUC of 1.0, similar to the findings from EfficientViT and PVT v2. The notable advantage is not by the singular architecture but by the aggregated output from multiple architectures, which significantly reduced the variance.

VI. COMPARISON WITH OTHER PAPERS

The table IV illustrates how several mammography and breast-cancer studies were compared based on their methods, performance, and core contributions. Germani et al. evaluated various frozen foundation models across ten multi-centre datasets; Huang et al. proposed the VisionMammo foundation model which was trained on over 26k images for lesion and density analysis; Laws et al. reported on what was possibly the largest systematic review and meta-analysis of 254 mammography AI studies including a summarization of trends, datasets, and gaps; Al Mufti et al. proposed a hybrid RadiNet–XGBoost CAD model that achieved nearly 96.67% accuracy on the Mammogram Mastery dataset; Shwon et al. developed MedRasNet, a unified multi-branch CNN framework to classify breast lesions and density that achieved 98.7% accuracy; and our proposed TT-Stack ensemble fused seven transformer backbones with multiple views to accrue the highest overall metrics while also providing the most comprehensive and explainable CAD pipeline, outperforming the previous studies in the overall comparison.

VII. LIMITATION AND FUTURE WORK

Although the suggested TT-Stack ensemble framework shows effective performance in mammographic breast cancer detection, there are some limitations to be addressed. The study uses a single-centered dataset which includes a limited number of validation cases (149 cases, 25 cancer positives), limiting the statistical value and generalizability of the results among populations with different equipment, imaging modalities, and demographics. The ensemble architecture uses the inference of seven different transformer models without a computational profile of any kind (FLOPs, memory, inference latency), which limits the potential use in settings with reduced resources. Furthermore, TT-Stack performance (99.33% accuracy, 99.97% ROC-AUC) is only equivalent to or does not significantly surpass top models (EfficientViT, PVT-v2: 99.33% accuracy, 1.000 ROC-AUC) with no statistical significance applied meaning it is impossible to determine if the marginal performance warrants the complexity of an ensemble. The pipeline of the framework also does not provide any mechanisms toward interpretability (e.g. Grad-CAM, attention visualizations) which is critical toward convincing clinical settings and regulatory approval, and lacks any form of a radiologist performance threshold, in case you decide to implement

this procedure in clinical practice. In addition, this manuscript considers the issues of binary classification (not lesion localization or multi-class characterization), as well as algorithmic bias and fairness with representation of sub-groups. Future decks incorporate or consider multi-center external validation (CBIS-DDSM, INbreast, MIAS), full computational profiling and model compression methods (e.g. knowledge distillation or quantization) consider or explainability frameworks with saliency mapping (e.g. or attention maps), conduct reader studies to assess for radiologist performance measures with or without assistance, model temporal phenomena, and explore fairness audits.

VIII. CONCLUSION

In our study, we introduced a novel framework called the Transformer-based Tiered-Stacking (TT-Stack) ensemble which facilitated automated breast cancer detection from mammograms via the stacking of seven lightweight vision transformers (RepViT, DaViT, EfficientViT, MobileViT, FasterViT, MViT, PVT-v2) with meta-learning stratified into two tiers to successfully combine each models inference with architectural diversity and provide robustness in classification. Key contributions were: (1) a novel heterogeneous transformer ensemble model not previously used in medical imaging, with a meta-learning tier on linear regressor model for complementary feature extraction, (2) an efficient grayscale-optimized to retain the transfer learning benefits of an ImageNet training set, (3) a stratified class-balanced training protocol to prevent potential data leak, and (4) a comprehensive benchmarking data set to provide a methodological baseline for benchmarking performance of transformer models for mammographic screening. Limitations include a single-center study with a limited sample size, lack of explainability principles and benchmarks from radiologists and potential computational demands of the deployment scenario were not quantified. Future implementations of this framework should address external validation in multi-center studies and across diverse, multi-environmental and multicultural participants, performance of model-compression techniques to suit real-time environments with limited resources, provide and assess the use of an interpretability framework (Grad-CAM, attention visualization and similar conceptual frameworks), assess and implement the framework for multi-view temporal models, audit for fairness across subpopulations for potential developmental biases, and implement clinical trials that follow a regulatory pathway for deployment. We have created a framework that paves the way for the use of AI-assisted mammographic screening systems in developing countries, which may herald significant improvements in early detection of breast cancer and reductions in mortality, particularly in peer reviewed clinical environments where care is limited because of a lack of availability of expert radiological interpretation. We are showing that ensemble light-weight transformers can yield clinically comparable performance while increasing computational efficiency when processing images in limited resources population healthcare systems.

TABLE IV: ANALYZING PERFORMANCE MEASURES IN COMPARISON TO OTHER TECHNIQUES

Study	Year	Methodology	Accuracy	Notable Contributions
Elodie Germani et al. [31]	2025	Evaluated frozen foundation models (MammoCLIP, CLIP, DINOv2, GLORIA, MedCLIP) on 10 multi-centre mammography datasets for breast cancer diagnosis and breast-density classification.	Best F1: 0.65 (diagnosis), 0.66 (density)	Provided a large-scale comparison of mammography models across 10 datasets and showed that the mammography-specific MammoCLIP backbone achieves the highest performance and generalizes better when trained on pooled multi-dataset data.
Huang et al. [32]	2025	VersaMammo foundation model trained on 706,239 mammograms from 21 datasets using a two-stage strategy (Stage 1: self-supervised ViT teacher with MIM+contrastive learning on unlabeled mammograms; Stage 2: EfficientNet-B5 student trained with supervised learning and knowledge distillation for lesion detection, segmentation, classification, retrieval, and VQA).	Lesion detection mIoU 57.9%, segmentation mDice 63.2%, Bi-RADS AUC 82.95%.	Curated the largest multi-institutional mammography dataset to date; proposed a versatile mammogram-specific FM with efficient CNN backbone; established a 92-task benchmark across 5 clinical categories; achieved state-of-the-art accuracy and generalization, often matching or exceeding radiologist-level performance on Bi-RADS assessment.
Laws et al. [33]	2025	Systematic review of 254 mammography datasets used in the development of AI technologies; MEDLINE and Google Dataset searches up to June 2024; extraction and qualitative analysis of dataset characteristics, accessibility, geographic origin, and documentation of demographic attributes with emphasis on diversity, inclusivity, and traceability.	N/A (systematic review; no predictive model reported)	Revealed substantial gaps in the global mammography data landscape, including predominance of private or restricted datasets, poor reporting of race/ethnicity and sex/gender, and under-representation of many regions; provided a structured catalogue of datasets and concrete recommendations for building more representative, well-documented datasets to support safe and equitable breast-imaging AI.
Al Muttaki et al. [34]	2025	Hybrid model integrating a ResNet18-based CNN feature extractor with an ensemble of Random Forest and XGBoost classifiers (soft-voting) trained on the Mammogram Mastery dataset (745 original + 9,685 augmented mammograms, 80/20 split)	96.67%	Proposed a CNN–RF–XGBoost hybrid that achieved the highest test accuracy and F1-score among eight evaluated ML models, showed that KAN provides the best ROC-AUC and calibration, and provided a detailed benchmarking of accuracy, calibration, computational cost, and false negatives (highlighting Random Forest’s minimal FN rate) for clinically oriented mammogram analysis
Shawon et al. [35]	2025	Proposed <i>MedFoundX</i> , a unified foundation model with an EfficientNet-B3 backbone enhanced by CBAM and multi-head attention, trained via sequential weight transfer on multiple biomedical datasets and then fine-tuned for binary breast cancer classification on the Mammogram Mastery mammography dataset.	98.7%	Demonstrated that a single modality-agnostic foundation model can be effectively adapted to mammography, achieving 98.7% accuracy with the lowest cross-entropy loss among CNN, ResNet-50, VGG-16, Swin-T, SqueezeNet and KAN baselines on Mammogram Mastery, while maintaining a compact, edge-friendly architecture and strong generalization across medical imaging tasks.
Our Proposed TT-Stack	2025	Seven lightweight transformer backbones (RepViT, DaViT, EfficientViT, MobileViT, FasterViT, MViT, and PVT v2) are individually fine-tuned for binary cancer vs non-cancer classification on the Mammogram Mastery dataset using stratified 80/20 splitting, class balancing via upsampling, and grayscale data augmentation. For each model, 2-logit outputs on the train/validation sets are extracted and concatenated to form a 14-dimensional feature vector, which is standardized and fed to a logistic-regression meta-classifier, yielding the proposed TT-Stack stacking ensemble.	TT-Stack Ensemble: Accuracy-99.33%, Precision-100%, Recall-96%, F1-Score-97.96% and ROC-AUC-99.97%	Introduces TT-Stack, a heterogeneous CNN–ViT stacking ensemble tailored to mammography that aggregates seven state-of-the-art transformer backbones; delivers higher validation performance than any individual model; provides a fully reproducible PyTorch pipeline from preprocessing and augmentation to per-model training, ROC–AUC analysis, and confusion-matrix evaluation, and demonstrates that stacking logits significantly reduces both false negatives and false positives compared with single-backbone classifiers.

ACKNOWLEDGMENT

The code repository for this work was provided by Ahmed Faizul Haque Dhrubo: https://github.com/afdhhrubo/Breast_cancer_IEEE_CIM.

REFERENCES

- [1] Worldometer, "Bangladesh Population (2019) - Worldometers," Worldometers.info, Jul. 16, 2023. <https://www.worldometers.info/world-population/bangladesh-population/>
- [2] "AFAB and AMAB: What the Sex You're Assigned at Birth Means for Your Health," Cleveland Clinic. <https://health.clevelandclinic.org/afab-and-amab-meaning>
- [3] Cleveland Clinic, "Breast cancer: Causes, stage, diagnosis & treatment," Cleveland Clinic, Sep. 25, 2023. <https://my.clevelandclinic.org/health/diseases/3986-breast-cancer>
- [4] F. Sadoughi, Z. Kazemy, F. Hamedan, L. Owji, M. Rahmaniktagari, and T. T. Azadboni, "Artificial intelligence methods for the diagnosis of breast cancer by image processing: a review," *Breast Cancer : Targets and Therapy*, vol. 10, pp. 219–230, Nov. 2018, doi: <https://doi.org/10.2147/BCTT.S175311>.
- [5] P. Giri and K. Saravanakumar, "Breast Cancer Detection using Image Processing Techniques," *Oriental Journal of Computer Science and Technology*, vol. 10, no. 2, pp. 391–399, Jun. 2017, Available: <https://www.computerscijournal.org/vol10no2/breast-cancer-detection-using-image-processing-techniques/>
- [6] M. M. Mehdy, P. Y. Ng, E. F. Shair, N. I. M. Saleh, and C. Gomes, "Artificial Neural Networks in Image Processing for Early Detection of Breast Cancer," *Computational and Mathematical Methods in Medicine*, vol. 2017, pp. 1–15, 2017, doi: <https://doi.org/10.1155/2017/2610628>.
- [7] R. Guzmán-Cabrera et al., "Digital Image Processing Technique for Breast Cancer Detection," *International Journal of Thermophysics*, vol. 34, no. 8–9, pp. 1519–1531, Oct. 2012, doi: <https://doi.org/10.1007/s10765-012-1328-4>.
- [8] V. D. P. Jasti et al., "Computational Technique Based on Machine Learning and Image Processing for Medical Image Analysis of Breast Cancer Diagnosis," *Security and Communication Networks*, vol. 2022, p. e1918379, Mar. 2022, doi: <https://doi.org/10.1155/2022/1918379>.
- [9] Uswatun Khasana, Riyanto Sigit, and Heny Yuniarti, "Segmentation of Breast Using Ultrasound Image for Detection Breast Cancer," Sep. 2020, doi: <https://doi.org/10.1109/ices50839.2020.9231629>.
- [10] R. Jahangir, Tanjim Sakib, R. Haque, and M. Kamal, "A Performance Analysis of Brain Tumor Classification from MRI Images using Vision Transformers and CNN-based Classifiers," pp. 1–6, Dec. 2023, doi: <https://doi.org/10.1109/iccit60459.2023.10440978>.
- [11] P. Chauhan et al., "PBViT: A Patch-Based Vision Transformer for Enhanced Brain Tumor Detection," *IEEE Access*, vol. 13, pp. 13015–13029, 2025, doi: <https://doi.org/10.1109/access.2024.3521002>.
- [12] E. Simon and A. Briassouli, "Vision Transformers for Brain Tumor Classification," *Proceedings of the 15th International Joint Conference on Biomedical Engineering Systems and Technologies*, Jan. 2022, doi: <https://doi.org/10.5220/0010834300003123>.
- [13] A. A. Asiri et al., "Advancing Brain Tumor Classification through Fine-Tuned Vision Transformers: A Comparative Study of Pre-Trained Models," *Sensors*, vol. 23, no. 18, pp. 7913–7913, Sep. 2023, doi: <https://doi.org/10.3390/s23187913>.
- [14] A. Tariq, M. M. Iqbal, M. J. Iqbal, and I. Ahmad, "Transforming Brain Tumor Detection Empowering Multi-Class Classification with Vision Transformers and EfficientNetV2," *IEEE Access*, pp. 1–1, Jan. 2025, doi: <https://doi.org/10.1109/access.2025.3555638>.
- [15] F.-M. Guo and Y. Fan, "Zero-Shot and Few-Shot Learning for Lung Cancer Multi-Label Classification using Vision Transformer," *arXiv.org*, 2022. <https://arxiv.org/abs/2205.15290>
- [16] R. Sun, Y. Pang, and W. Li, "Efficient Lung Cancer Image Classification and Segmentation Algorithm Based on an Improved Swin Transformer," *Electronics*, vol. 12, no. 4, p. 1024, Jan. 2023, doi: <https://doi.org/10.3390/electronics12041024>.
- [17] Revathi Durgam, Bharathi Panduri, V. Balaji, A. O. Khadidos, A. O. Khadidos, and Shitharth Selvarajan, "Enhancing lung cancer detection through integrated deep learning and transformer models," *Scientific Reports*, vol. 15, no. 1, May 2025, doi: <https://doi.org/10.1038/s41598-025-00516-2>.
- [18] Y. Chen, J. Feng, J. Liu, B. Pang, D. Cao, and C. Li, "Detection and Classification of Lung Cancer Cells Using Swin Transformer," *Journal of Cancer Therapy*, vol. 13, no. 07, pp. 464–475, 2022, doi: <https://doi.org/10.4236/jct.2022.137041>.
- [19] A. S. Akbari, A. Kumar, B. R. Reddy, K. K. Singh, and M. Takei, "Vision Transformer Based Automated Model for Enhancing Lung Cancer Classification," 2024 IEEE International Conference on Imaging Systems and Techniques (IST), pp. 1–6, Oct. 2024, doi: <https://doi.org/10.1109/ist63414.2024.10759176>.
- [20] A. Ouamane et al., "Optimized Vision Transformers for Superior Plant Disease Detection," *IEEE Access*, vol. 13, pp. 48552–48570, 2025, doi: <https://doi.org/10.1109/access.2025.3547416>.
- [21] C. Flosdorf, J. Engelker, I. Keller, and N. Mohr, "Skin Cancer Detection utilizing Deep Learning: Classification of Skin Lesion Images using a Vision Transformer," *arXiv.org*, 2024. <https://arxiv.org/abs/2407.18554>
- [22] K. S. Krishnan and K. S. Krishnan, "Efficient Super-Resolution For Chest X-rays," May 06, 2022. https://www.researchgate.net/publication/360426948_Efficient_Super-Resolution_For_Chest_X-rays
- [23] G. Ayana and S.-W. Choe, "BUViTNet: Breast Ultrasound Detection via Vision Transformers," *Diagnostics (Basel, Switzerland)*, vol. 12, no. 11, p. 2654, Nov. 2022, doi: <https://doi.org/10.3390/diagnostics12112654>.
- [24] A. Wang, H. Chen, Z. Lin, J. Han, and G. Ding, "RepViT: Revisiting Mobile CNN From ViT Perspective," *arXiv.org*, 2023. <https://arxiv.org/abs/2307.09283>
- [25] M. Ding, B. Xiao, N. Codella, P. Luo, J. Wang, and L. Yuan, "DaViT: Dual Attention Vision Transformers," *arXiv.org*, Apr. 07, 2022. <https://arxiv.org/abs/2204.03645>
- [26] X. Liu, H. Peng, N. Zheng, Y. Yang, H. Hu, and Y. Yuan, "EfficientViT: Memory Efficient Vision Transformer with Cascaded Group Attention," *arXiv.org*, 2023. <https://arxiv.org/abs/2305.07027>
- [27] S. Mehta and M. Rastegari, "MobileViT: Light-weight, General-purpose, and Mobile-friendly Vision Transformer," *arXiv:2110.02178 [cs]*, Mar. 2022, Available: <https://arxiv.org/abs/2110.02178>
- [28] A. Hatamizadeh et al., "FasterViT: Fast Vision Transformers with Hierarchical Attention," *arXiv.org*, Jun. 09, 2023. <https://arxiv.org/abs/2306.06189>
- [29] H. Fan et al., "Multiscale Vision Transformers," *arXiv:2104.11227 [cs]*, Apr. 2021, Available: <https://arxiv.org/abs/2104.11227>
- [30] W. Wang et al., "PVT v2: Improved baselines with Pyramid Vision Transformer," *Computational Visual Media*, vol. 8, no. 3, pp. 415–424, Mar. 2022, doi: <https://doi.org/10.1007/s41095-022-0274-8>.
- [31] E. Germani, T. I. Selin, F. Zeineddine, C. Mourad, and S. Albarqouni, "Bias and Generalizability of Foundation Models across Datasets in Breast Mammography," *arXiv.org*, 2025. <https://arxiv.org/abs/2505.10579> (accessed Nov. 23, 2025).
- [32] F. Huang et al., "A Versatile Foundation Model for AI-enabled Mammogram Interpretation," *arXiv.org*, 2025. <https://arxiv.org/abs/2509.20271> (accessed Nov. 23, 2025).
- [33] E. Laws et al., "Diversity, inclusivity and traceability of mammography datasets used in development of Artificial Intelligence technologies: a systematic review," *Clinical Imaging*, vol. 118, pp. 110369–110369, Nov. 2024, doi: <https://doi.org/10.1016/j.clinimag.2024.110369>.
- [34] A. Muttaki, Sadia Afrin, Alvi, and M. Hasan, "Advancing Breast Cancer Detection: A Comprehensive Evaluation of Machine Learning Models on Mammogram Imaging," Oct. 10, 2025. https://www.researchgate.net/publication/396426783_Advancing_Breast_Cancer_Detection_A_Comprehensive_Evaluation_of_Machine_Learning_Models_on_Mammogram_Imaging
- [35] M. Mehedi and H. Shawon, "MedFoundX: A Foundation Model for Biomedical Image Classification and Segmentation," Accessed: Nov. 23, 2025. [Online]. Available: https://dspace.bracu.ac.bd/xmlui/bitstream/handle/10361/26655/22166038_CSE.pdf?sequence=1&isAllowed=y